IOPscience iopscience.iop.org

Home Search Collections Journals About Contact us My IOPscience

Fluxons in a superlattice of Josephson junctions: dynamics and radiation

This article has been downloaded from IOPscience. Please scroll down to see the full text article.

2003 J. Phys. A: Math. Gen. 36 2423

(http://iopscience.iop.org/0305-4470/36/10/304)

View the table of contents for this issue, or go to the journal homepage for more

Download details:
IP Address: 171.66.16.96
The article was downloaded on 02/06/2010 at 11:27

Please note that terms and conditions apply.

INSTITUTE OF PHYSICS PUBLISHING JOURNAL OF PHYSICS A: MATHEMATICAL AND GENERAL

J. Phys. A: Math. Gen. **36** (2003) 2423–2441 PII: S0305-4470(03)57314-0

Fluxons in a superlattice of Josephson junctions: dynamics and radiation

Y Gaididei[1], **N Lazarides**[2] **and N Flytzanis**[3]

[1] Institute for Theoretical Physics, 252143 Kiev, Ukraine
[2] Department of Materials Science and Technology, University of Crete, PO Box 2208, 71003 Heraklion, Greece
[3] Physics Department, University of Crete, PO Box 2208, 71003 Heraklion, Greece

Received 6 December 2002
Published 26 February 2003
Online at stacks.iop.org/JPhysA/36/2423

Abstract

We study the dynamics of a homopolar coherent array of fluxons in a planar superlattice of long Josephson junctions coupled through lateral idle regions. These regions introduce dispersion, which in effect destroys the Lorentz invariance of the usual sine-Gordon equation. Thus, the system is described by an effectively non-local equation. We use a collective coordinate approach to determine the fluxon width resulting uniform coherent fluxon motion, as well as the fluttering frequency as a function of the momentum, which is an integral of the motion. At relatively high fluxon velocities Cherenkov radiation appears as oscillations following the propagating fluxon. We obtained analytical formulae for the wavevector, frequency, amplitude and form of the emitted radiation. The analytical results are in fair agreement with numerical simulations. At very high fluxon velocities, the radiation strongly modifies the I–v characteristics leading to resonant structures, known as Cherenkov steps. The coherency of the emitted radiation makes possible the use of such devices as rf oscillators in the gigahertz region, where they can compete with semiconductor based oscillators.

PACS numbers: 74.50.+r, 74.60.Jg

1. Introduction

One of the important characteristics of Josephson junctions is that when they are biased in a zero field step (ZFS), an ac signal in the microwave range is obtained. The emitted power is usually small unless phase locking of several junctions is achieved [1, 2]. In this case the power due to radiation goes as the square of the number of junctions (N^2), while the linewidth decreases as $1/N$. Therefore a great deal of effort has been devoted to demonstrate experimentally the possibility of mutual synchronization in stacked junctions [3, 4] and in arrays of short [5, 6] and long [2, 7–9] Josephson junctions.

 © 2003 IOP Publishing Ltd Printed in the UK

The geometry of a parallel array of coupled long junctions is of interest because fluxon excitations in neighbouring junctions are attracted [8], so that coherent phase-locked propagation of fluxons can be achieved. In a previous work, the static coherent fluxon solution has been found analytically for a planar array of long junctions coupled through intermediate regions where there is no Josephson and quasiparticle tunnelling (idle regions) [16]. These regions can also be thought of as long columnar defects in a large area junction [9]. Devices of this type can be easily fabricated with Nb electrodes, using photolithographic patterning and deposition by thermal evaporation of SiO and lift off before depositing the top electrode layer [9].

The idle regions severely affect the static as well as the dynamic behaviour of fluxons. The fluxon's width increases with increasing size of the idle regions, and therefore becomes less effective in screening an external magnetic field [10]. In effect, the first critical field H_{c1} decreases with increasing idle regions, showing good agreement with the experiments [11]. At the same time the idle regions introduce dispersion due to the curved paths of current through the idle regions, thus the term non-locality. In effect the maximum fluxon velocity increases with increasing idle regions, until it reaches a saturation velocity. For relatively high velocities, we also have the possibility of Cherenkov radiation. This is important, since through this mechanism we could get radiation of greater frequency which depends on the driving current and can be continuously varied [12]. Evidence for Cherenkov radiation of fluxons has been observed in stacks of annular junctions [13, 14], and in an intrinsic stack of long Josephson junctions, i.e., a naturally layered high-T_c superconductor [15].

In this paper we study the dynamics of a coherent fluxon array using analytical and numerical results. In section 2 we present the model of a periodic superlattice of Josephson junctions in the limit of long narrow windows, while in section 3 we use a collective coordinate ansatz to describe the dynamics of a coherent homopolar array of coupled fluxons. In section 4 we discuss the problem of radiation, and in section 5 we present numerical results showing Cherenkov steps on the first ZFS. We finish in section 6 with conclusions.

2. Model and equations of motion

We consider a planar parallel array of long Josephson junctions, which can be implemented by periodic variation of the oxide width, $d(x)$, in the x-direction [16]. Limiting ourselves to $d(x) \ll \lambda_L$, where λ_L is London penetration depth, we can assume that there is no variation of the magnetic thickness and therefore of the inductance along x. We consider that $d(x)$ is varied as

$$d(x) = \begin{cases} d_j & \text{if} \quad |x - \ell n| < \dfrac{w}{2} \quad n = 0, \pm 1, \pm 2, \dots \\ d_i & \text{otherwise} \end{cases} \tag{1}$$

with $d_i \gg d_j$, so that the critical Josephson current as well as the quasiparticle current practically vanish in the idle region (where $d(x) = d_i$), since they are both exponentially sensitive on $d(x)$. Thus we end up with a periodic planar array of active (with tunnelling) and passive (with no tunnelling) waveguides, shown schematically in figure 1. The strong variation of $d(x)$ influences strongly the local speed of electromagnetic waves, v. Since $v \propto d(x)$, and $d_i \gg d_j$, hence $v_i \gg v_j$, where v_j and v_i are the wave velocities in the active and idle regions, respectively. For simplicity we can take $v_i \to \infty$. For the case of narrow junctions, the electromagnetic properties of this system are well described by the following equation [16]:

$$\left[\partial_x^2 + \partial_z^2 - \frac{w}{v_j^2} f(x) \partial_t^2\right] \phi = \frac{w}{\lambda_j^2} f(x) \sin \phi \tag{2}$$

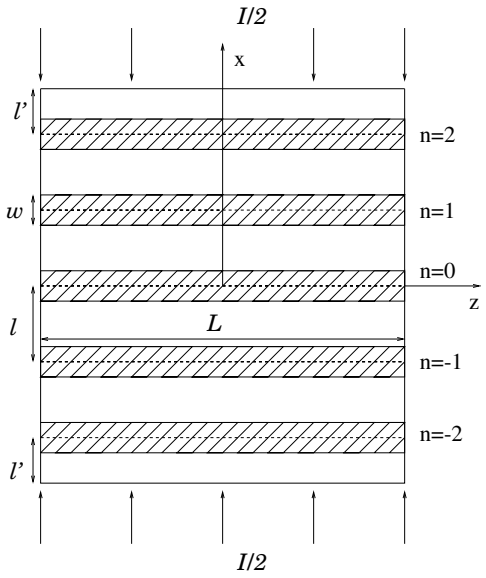

Figure 1. Schematic planar view of a Josephson junction superlattice.

where $\partial_x \equiv \frac{\partial}{\partial x}$, etc, λ_j is the Josephson penetration depth in the junction and $f(x)$ is the structure function

$$f(x) = \sum_n \delta(x - x_n) \tag{3}$$

with $x_n = n\ell, n = 0, \pm 1, \pm 2, \ldots$. In equation (2) we have shrunk the junction windows to a delta function, but we also scaled the critical current density by the junction width w, so that the integrated current remains the same. We also assume that within the width w the phase ϕ does not vary significantly, and we can define an average phase $\Phi_n(z, t)$ of the nth junction as

$$\Phi_n(z, t) = \frac{1}{w} \int_{-\frac{w}{2}}^{\frac{w}{2}} \mathrm{d}x\, \phi(x, z, t) \tag{4}$$

and for small w we can also write

$$\sin \Phi_n(z, t) = \frac{1}{w} \int_{-\frac{w}{2}}^{\frac{w}{2}} \mathrm{d}x \sin \phi(x, z, t). \tag{5}$$

Equation (2) is linear everywhere except along the junctions, where the non-linearity comes in. Thus using the Fourier transform of $\phi(x, z, t)$ as

$$\phi(x, z, t) = \int_{-\infty}^{\infty} \mathrm{d}k\, \bar{\phi}(x, k, t)\, \mathrm{e}^{\mathrm{i}kz} \tag{6}$$

where the bar distinguishes the Fourier transformed quantity, we can solve the corresponding Laplace equations [16, 17] in the linear region. The arbitrary coefficients are determined through the boundary conditions at the junction edges, as a function of the phases Φ_n on the junctions. Integrating equation (2) over x in the range

$$n\ell - \frac{w}{2} \leqslant x \leqslant n\ell + \frac{w}{2}$$

and using the definitions given by equations (4) and (5), we get

$$\partial_x \phi \,|_{n\ell-0}^{n\ell+0} - \frac{1}{v_j^2}\Phi_n = \frac{1}{\lambda_j^2}\sin\Phi_n. \tag{7}$$

The discontinuity in the derivative $\partial_x\phi$ across $x = n\ell$ can be evaluated through the boundary conditions as a function of the phase Φ_n and the phases of the neighbouring junctions, Φ_{n+1} and Φ_{n-1}. Then, after extensive calculations we obtain a set of coupled non-local equations [16], which can be represented in an operator form as

$$\frac{\hat{k}}{\sinh \ell\hat{k}}(\Phi_{n+1} + \Phi_{n-1}) - 2\frac{\hat{k}}{\tanh \ell\hat{k}}\Phi_n - \frac{w}{v_j^2}\partial_t^2\Phi_n = \frac{w}{\lambda_j^2}\sin\Phi_n \tag{8}$$

for $n = 0, \pm1, \pm2, \ldots$. The operator $\hat{k} \equiv \mathrm{i}\partial_z$ can be defined by its Fourier transform

$$\overline{\hat{k}\Phi}(k,t) = \frac{1}{2\pi}\int_{-\infty}^{\infty} \mathrm{d}z\, \mathrm{e}^{-\mathrm{i}kz}\, \mathrm{i}\partial_z\Phi_n(z,t) = k\overline{\Phi_n}(k,t). \tag{9}$$

Using the Fourier transform of Φ_n (equation (6)), we can rewrite equation (8) in integral form as

$$\begin{aligned}\frac{w}{\lambda_j^2}\sin\Phi_n(z,t) + \frac{w}{v_j^2}\partial_t^2\Phi_n(z,t) &= \frac{2}{\pi}\int_{-\infty}^{\infty}\mathrm{d}\zeta\, \ln\left[\coth\left(\frac{\pi}{2\ell}|\zeta - z|\right)\right]\partial_\zeta^2\Phi_n(\zeta,t) \\ &+ \frac{\pi}{4\ell^2}\int_{-\infty}^{\infty}\mathrm{d}\zeta\, \mathrm{sech}^2\left[\frac{\pi}{2\ell}(\zeta - z)\right][\Phi_{n+1}(\zeta,t) + \Phi_{n-1}(\zeta,t) - 2\Phi_n(\zeta)]\end{aligned} \tag{10}$$

so that the non-local character of the equations is more apparent than when these are expressed with the pseudodifferential operators in equation (8). The non-locality is only in space since the velocity of the waves in the idle region is infinite so that the variation of the phase in the window is transferred instantly at every point in the idle region. Thus the only variation with time in $\phi(x,z,t)$ in the idle region comes through the time variation of $\Phi_n(z,t)$ in the window. The non-locality in space means that the supercurrent at each point is not a local property of the phase but depends on the current at any other point, which in fact can follow a curved trajectory between the two points. Once the system of equations (8) is solved for the phases $\Phi_n(z,t)$, we can evaluate the phase $\phi(x,z,t)$ everywhere from [16]

$$\phi(x,z,t) = \frac{\sinh(\hat{k}((n+1)\ell - x))}{\sinh(\hat{k}\ell)}\Phi_n(z,t) + \frac{\sinh(\hat{k}(x - n\ell))}{\sinh(\hat{k}\ell)}\Phi_{n+1}(z,t) \tag{11}$$

for $n\ell \leqslant x \leqslant (n+1)\ell$, $n = 0, \pm1, \pm2, \ldots$, and from the definition (4) at $x = n\ell$ and $x = (n+1)\ell$ it is equal to $\Phi_n(z,t)$ and $\Phi_{n+1}(z,t)$, correspondingly.

A solution of particular interest is when we have coherent motion of fluxons, with $\Phi_n(z,t) = \Phi(z,t)$ for all n. Then the function $\Phi(z,t)$ satisfies the non-local sine-Gordon (sG) equation

$$\frac{w}{v_j^2}\partial_t^2\Phi + 2\hat{k}\tanh\frac{\ell\hat{k}}{2}\Phi = -\frac{w}{\lambda_j^2}\sin\Phi \tag{12}$$

or in its integral form

$$\frac{w}{v_j^2}\partial_t^2\Phi(z,t) - \frac{2}{\pi}\int_{-\infty}^{\infty}\mathrm{d}\zeta\, \ln\left[\coth\left(\frac{\pi}{2\ell}|\zeta - z|\right)\right]\partial_\zeta^2\Phi(\zeta,t) = -\frac{w}{\lambda_j^2}\sin\Phi(z,t). \tag{13}$$

In the limit of infinitely distant junctions ($\ell \to \infty$), we get the sine-Hilbert equation [18, 19] which admits an analytic solution of the travelling wave type. Similar kernels also arise in non-local sG-type equations with a different physical mechanism as their origin [20–24].

Equation (12) which describes the dynamics of coherent fluxons can be obtained as the Euler–Lagrange (EL) equation from the action

$$S = \int_{-\infty}^{\infty} \mathrm{d}t\, \mathcal{L}(t) \tag{14}$$

where

$$\mathcal{L} = \int_{-\infty}^{\infty} \mathrm{d}z \left[\frac{1}{2}\frac{w}{v_j^2}(\partial_t \Phi)^2 - \Phi \hat{k} \tanh \frac{\ell \hat{k}}{2}\Phi - \frac{w}{\lambda_j^2}(1-\cos\Phi) \right] \tag{15}$$

is the Lagrange function of the system. In the next section we study the fluxon dynamics using a variational (collective coordinate) approach.

3. Dynamics of Josephson vortices

In the spirit of the collective coordinate approach, we describe the fluxon form in terms of two macroscopic parameters with physical significance, i.e. the fluxon position and the fluxon width which can vary with time during the fluxon motion. Guided by the analytical solution in the static limit of equation (12) [16, 18], we use as a trial function a time-dependent extension of the static solution

$$\Phi(z,t) = 4\arctan\left\{ \sec\left[\frac{\beta(t)}{2}\right] \sinh\left[\frac{\beta(t)}{\ell}(z - Z(t))\right] + \sqrt{\sec^2\left[\frac{\beta(t)}{2}\right] \sinh^2\left[\frac{\beta(t)}{\ell}(z - Z(t))\right] + 1} \right\} \tag{16}$$

where $\beta(t)$ describes the internal dynamics of the fluxon width, while $Z(t)$ characterizes the centre of the fluxon motion. The partial differential equations that describe the dynamics are transformed into ordinary differential equations for the collective coordinates $\beta(t)$ and $Z(t)$ through the effective Lagrangian

$$\mathcal{L} = T - U \tag{17}$$

where (as shown in the appendix)

$$T = \tfrac{1}{2} m(\beta)\dot{\beta}^2 + \tfrac{1}{2} M(\beta)\dot{Z}^2 \tag{18}$$

is the effective kinetic energy and

$$U = \frac{2w\ell}{\lambda_j^2}\cot\frac{\beta}{2} + 2\pi \int_0^{\infty} \mathrm{d}k \frac{\sinh\frac{2\beta}{\pi}k}{k\cosh^2 k} \tag{19}$$

is the potential energy. The effective masses of internal motion, $m(\beta)$, and fluxon position, $M(\beta)$, are a function of the width parameter β and are given by

$$m(\beta) = \frac{\pi^2}{3}\frac{w\ell}{v_j^2}\left[1 + \left(1 + 2\frac{\beta^2}{\pi^2}\right)\frac{\beta}{\sin\beta}\right]\frac{1}{\beta^3} \tag{20}$$

$$M(\beta) = 4\frac{w}{\ell v_j^2}\beta\left(1 + \frac{\beta}{\sin\beta}\right). \tag{21}$$

The effective kinetic and potential energies are measured in units of $\Phi_0^2/\mu_0 d_m$, where Φ_0 is the flux quantum and $d_m \simeq 2\lambda_{\mathrm{L}}$ is the magnetic thickness so that $\mathcal{L} = \mu_0 d_m$ is the inductance per

unit length (along z) of the junction. The effective kinetic energy of the system arises from the displacement current, and the capacitance per unit length is included in the velocity v_j. The potential energy is the magnetic energy in the whole superlattice and the Josephson energy in the windows. Since from the definition (16), $\beta(t)$ is dimensionless while $Z(t)$ has units of length, $m(\beta)$ is in units of time squared and $M(\beta)$ is in units of inverse squared velocity.

Looking at the Lagrangian we see that Z is a cyclic coordinate, which means that the corresponding generalized momentum is conserved. The EL equations for the coordinates $q = \beta$ or Z are obtained from

$$\frac{\mathrm{d}}{\mathrm{d}t}\frac{\partial \mathcal{L}}{\partial \dot{q}} = \frac{\partial \mathcal{L}}{\partial q}. \tag{22}$$

Then for $q = Z$ we get that the generalized momentum

$$P = \partial \mathcal{L}/\partial \dot{Z} = M(\beta)\dot{Z} \tag{23}$$

is a constant, with $M(\beta)$ given by equation (21). Thus we can eliminate $\dot{Z}$ from $\mathcal{L}$ in favour of P and obtain a new effective Lagrangian

$$\mathcal{L}_{\mathrm{eff}} = \mathcal{L} - P\dot{Z} = \frac{1}{2}m(\beta)\dot{\beta}^2 - U - \frac{P^2}{2}\frac{v_j^2 \ell \sin\beta}{4w\beta(\beta + \sin\beta)} = \frac{1}{2}m(\beta)\dot{\beta}^2 - U_{\mathrm{eff}} \tag{24}$$

where the effective potential

$$U_{\mathrm{eff}} = U + \frac{\ell P^2}{8w\beta}\frac{v_j^2 \sin\beta}{(\beta + \sin\beta)} \tag{25}$$

takes into account the coupling between the internal motion and the centre of fluxon motion expressed by equation (23).

The minimum of the effective potential, U_{eff}, with $P \neq 0$, corresponds to a uniformly moving fluxon with constant width and velocity. The fluxon width ℓ/β depends on the momentum P and its value is obtained from the position of the minimum of U_{eff}, which is determined by the equation (see the appendix)

$$2\beta \tan\left(\frac{\beta}{2}\right) - \frac{P^2c^2}{8}\frac{\sin^2\beta + 2\beta\sin\beta - \beta^2\cos\beta}{\beta^2(\beta + \sin\beta)^2}\sin^2\frac{\beta}{2} = \nu \tag{26}$$

where $c = v_j\sqrt{\frac{\ell}{w}}$ is the velocity of linear waves in the structure, and $\nu = \frac{w\ell}{\lambda_j^2}$ is the non-locality parameter. Note that for $P = 0$ equation (26) reduces to

$$2\beta_{\mathrm{s}} \tan\left(\frac{\beta_{\mathrm{s}}}{2}\right) = w\ell \equiv \nu \tag{27}$$

which determines the width of a static fluxon. A reasonably good approximation for $\beta_{\mathrm{s}}(w, \ell)$ is given by the simple interpolation formula [16]

$$\beta_{\mathrm{s}} = \frac{\pi}{\sqrt{1 + \frac{\pi^2}{w\ell}}} \tag{28}$$

which, for $\nu = w\ell \ll 1$, gives $\beta \simeq \sqrt{w\ell}$.

In the interval $\beta \in [0, \pi]$ equation (26) has only one solution for any value of P and ν. But the velocity $v = \dot{Z}$ of the uniform fluxon motion given by the expression

$$v(\beta) = c\cos\left(\frac{\beta}{2}\right)\sqrt{2\frac{2\beta\tan\left(\frac{\beta}{2}\right) - \nu}{\sin^2\beta + 2\beta\sin\beta - \beta^2\cos\beta}} \tag{29}$$

is a non-monotonic function of β with a maximum in the interval $[\beta_{\mathrm{s}}, \pi]$ where β_{s} is the solution of equation (26) in the case of an immobile fluxon ($P = 0$). The shape of $v(\beta)$ is

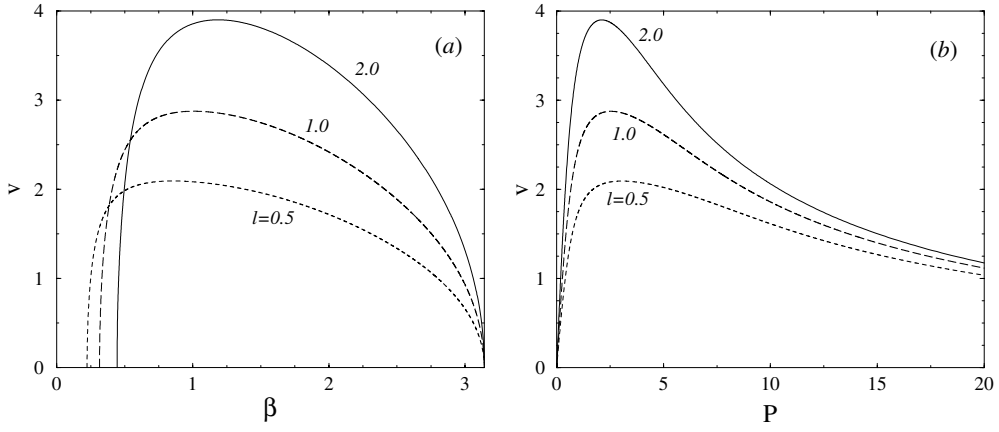

Figure 2. (*a*) The shape of the fluxon velocity v versus β for $w = 0.1$ and $\ell = 0.5$ (dashed curve), $\ell = 1.0$ (long-dashed curve), $\ell = 2.0$ (solid curve). The stable part in all cases is to the left of the maximum velocity. (*b*) The fluxon velocity v versus the momentum P for w and ℓ as in (*a*).

shown in figure 2(*a*) for $w = 0.1$ and $\ell = 0.5, 1.0, 2.0$. We see that v starts increasing from zero at β_s on the left, reaches a maximum velocity v_m, and then decreases to zero again at $\beta = \pi$. However, only the parts of the curves to the left of v_m correspond to a stable fluxon. Thus, we also find here a limiting velocity, which limits the applicability of the collective coordinate approach. In all cases v_m is less than the effective velocity c, which is an increasing function of the idle region width ℓ. It is however larger than v_j due to the fact that the tail of the fluxon hanging into the idle region tends to travel at higher velocities, and the critical velocity for linear waves in this compound superlattice is c.

The position of the maximum velocity, β_m, and its value, v_m, depend on the non-locality parameter ν. It is seen from equations (26) and (29) that the fluxon velocity is also a non-monotonic function of P (see figure 2(*b*)), i.e. $v(P)$ is double valued. We should notice here the peculiar situation that as the fluxon momentum increases, its velocity decreases to the right of the maximum. This is because $M(\beta)$ increases linearly with β for $v < v_m$ while for $v > v_m$ it increases as a higher power of β.

In figure 3(*a*) we plot β (actually its equilibrium value, β_p) as a function of P. The $\beta(P)$ curve starts from the static value, β_s, defined by equation (27) and rises almost quadratically up to the point where the velocity reaches a maximum. After that it increases more slowly until it levels at $\beta = \pi$. The range of stable solutions corresponds, however, to values of β far from π. In fact the arrows show the maximum value for each ℓ. In the limit of small non-locality ($\nu \ll 1$), we obtain from equation (29) that the maximum velocity v_m, its position β_m and the corresponding momentum P_m are given by

$$\beta_m^2 \simeq \sqrt{12\nu} \qquad v_m \simeq c \qquad P_m \simeq \frac{8\beta_m}{c} \to \sqrt{\frac{w}{\ell}}\frac{(\ell w)^{1/4}}{v_j}. \tag{30}$$

In figure 3(*b*) we see that the simple formula (30) for $\beta_m(\ell)$ is a good approximation over a large range of ℓ.

When the momentum P and/or the non-locality parameter ν become large, the solution of equation (26) takes the form

$$\beta = \pi - \frac{4\pi}{\ell}\left(\frac{w}{\lambda_j^2} + \frac{P^2 v_j^2}{8\pi^2 w}\right)^{-1} \tag{31}$$

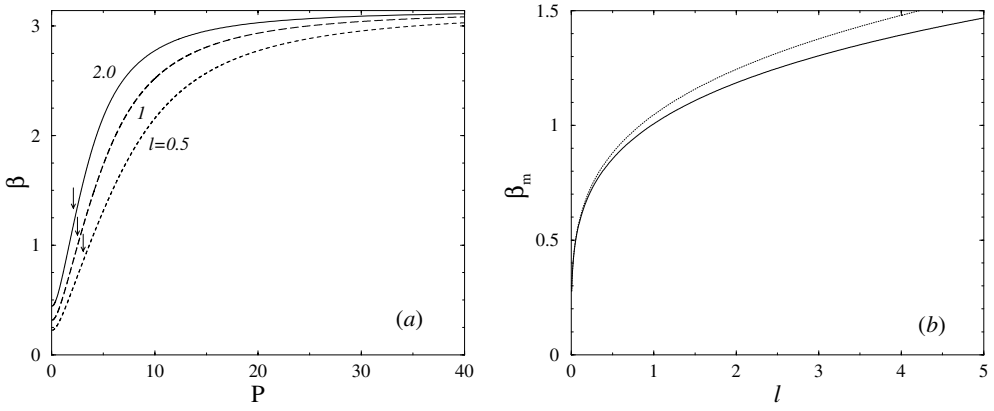

Figure 3. (*a*) The equilibrium value for β (i.e. β_p) versus the momentum P for w and ℓ as in figure 2. The stable range is to the left of the arrows. (*b*) The value of β where the velocity v is maximum, $\beta_{\rm m}$, versus the idle region width ℓ, for $w = 0.1$, calclulated from equation (29) (solid curve), along with the approximate formula $\beta_{\rm m}^2 \simeq \sqrt{12v}$ (dotted curve).

and the dependence of the fluxon velocity on the momentum can be written as

$$v(P) = 8\pi \frac{P v_j^2 \lambda_j^2}{8\pi^2 w^2 + P^2 v_j^2 \lambda_j^2}. \tag{32}$$

The function in equation (32) has a maximum at $P = 2\pi\sqrt{2}\frac{w}{\lambda_j v_j}$ with a maximum velocity $v_{\rm m} = \sqrt{2}\frac{v_j \lambda_j}{w}$.

Thus the momentum is the important parameter. For a fixed value of P, we can determine the corresponding value of β from equation (26). Then using either equation (29) or equation (23), we can determine the fluxon velocity. This prescription gives a single valued behaviour for both the fluxon width (ℓ/β) and the velocity $(\dot{Z})$ as a function of the momentum P.

When the width of the fluxon at $t = 0$ is not the one obtained from the minimum of $U_{\rm eff}$ ($\beta(t = 0) \neq \beta_p$), its dynamics will be described by the corresponding EL equation for β

$$\frac{1}{2} m'(\beta)\dot{\beta}^2 + m(\beta)\ddot{\beta} = -\frac{\partial U_{\rm eff}}{\partial \beta} \tag{33}$$

where $m'(\beta) = \frac{\partial m}{\partial \beta}$. This equation describes the fluttering phenomena around a moving fluxon. Rearranging the various terms in equation (33), we get

$$\ddot{\beta} = -\frac{1}{2} c(\beta)\dot{\beta}^2 - \frac{1}{m(\beta)} \frac{\partial U_{\rm eff}}{\partial \beta} \tag{34}$$

where $c(\beta) = m'(\beta)/m(\beta)$, and the explicit expressions for $m'(\beta)$ and $c(\beta)$ are given in the appendix.

A question that arises is how the static fluxon evolves if it has a width different from its static value $\beta_{\rm s}$ and second whether for β values different from $\beta_{\rm s}$, the analytic expression given in equation (16) as a function of β is still a good approximation when β is close to $\beta_{\rm s}$. The answer to the second question is also useful when we want to take into account the effect of velocity on the fluxon width in the case of a fluxon with finite momentum. So we consider small deviations of β from the equilibrium value β_p and examine its time evolution. The particle corresponding to the effective mass $m(\beta)$ with $\beta = \beta_p$ is still inside a well which

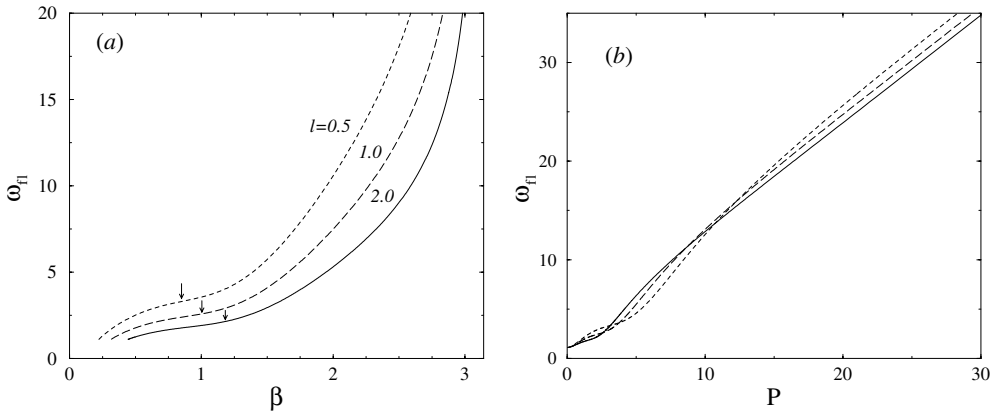

Figure 4. The fluttering frequency $\omega_{\rm fl}$: (a) versus $\beta = \beta_p$ and (b) versus the momentum P, for w and ℓ as in figure 2. In (a) the stable range is to the left of the arrows.

however is very steep on one side but for small deviations is harmonic. Then it can be shown that the width oscillates around β_p with a frequency given by

$$\omega_{\rm fl} = \sqrt{\frac{U''_{\rm eff}(\beta_p)}{m(\beta_p)}} \tag{35}$$

where $U''(\beta_p)$ is the second derivative of the effective potential in equation (25) with β evaluated at its equilibrium point β_p. The frequency $\omega_{\rm fl}$ is called the fluttering frequency and as a result of this the fluxons have an oscillating width so that they have a breathing-like mode.

In the case $P = 0$ the fluttering frequency is determined by the expression

$$\omega_{\rm fl}^2 = \frac{1}{m(\beta_{\rm s})}\frac{{\rm d}^2U}{{\rm d}\beta^2}\bigg|_{\beta_{\rm s}} = \frac{12}{\pi^2\nu}\frac{1}{\sin\beta_{\rm s}}\frac{\beta_{\rm s}^3(\beta_{\rm s}+\sin\beta_{\rm s})}{\sin\beta_{\rm s}+\left(1+2\frac{\beta_{\rm s}^2}{\pi^2}\right)\beta_{\rm s}} \tag{36}$$

where $\beta_{\rm s}$ is the solution of equation (26) at $P = 0$. In the limit of small ℓ (and β), we can obtain

$$\omega_{\rm fl}^2 \simeq \frac{12}{\pi^2} \qquad \text{as} \quad \nu \to 0 \tag{37}$$

while in the other extreme

$$\omega_{\rm fl}^2 \simeq \frac{1}{w^2} \qquad \text{as} \quad \nu \to \infty. \tag{38}$$

In figure 4(a) we plot $\omega_{\rm fl}$ as a function of β_p while in figure 4(b) we plot $w_{\rm fl}$ as a function of the momentum P. We see that at $P = 0$ or $\beta = \beta_{\rm s}$, $\omega_{\rm fl} \simeq 1.1$ (independent of ℓ for small ν), which is very close to the value predicted by equation (37). In fact this value has also been verified in the simulations for a static fluxon by choosing an initial value for β slightly different from $\beta_{\rm s}$. The simple result in equation (37) is a good approximation even for higher ν values. This can be understood since in a large range of interest, $\beta \ll \pi$ and therefore corrections are in powers of β/π. The useful range of the plot is again indicated by arrows for figure 4(a), while in figure 4(b) the useful range is in the corner for $P \lesssim 2$. In figures 5(a) and (b) we show the effective masses $m(\beta)$ and $M(\beta)$ as a function of the fluxon momentum, P. We see that for small momentum m is a strongly decreasing function of momentum. It starts from $\frac{3\pi^2}{2}\beta_{\rm s}$ and for $P \simeq 2$, it is comparable to $M(P)$. This means

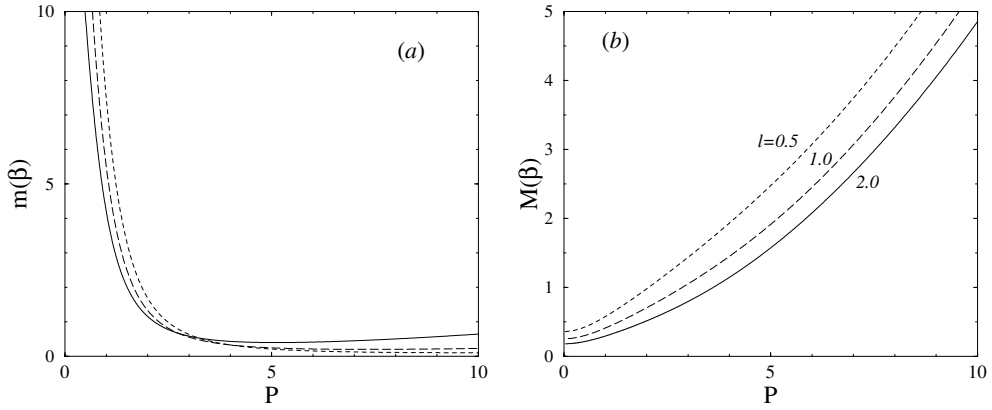

Figure 5. The effective masses (*a*) $m(\beta)$ and (*b*) $M(\beta)$ versus the fluxon momentum P, with w and ℓ as in figure 2.

that at low translational momentum, it is very difficult to excite width oscillations, while for larger values of momentum both degrees of freedom are important. Near $P \simeq 0$ the mass $m(\beta)$ behaves as

$$m(\beta) \simeq m_0 \sqrt{1 - \left(\frac{P}{M_0 c}\right)^2}$$

where $m_0 = m(\beta_s)$. In contrast $M(P)$ is an increasing function of momentum. At $P = 0$ and $\beta = \beta_s$, we have

$$M(\beta) \simeq \frac{8w}{\ell v_j^2}\sqrt{v} = \frac{0.264}{\sqrt{\ell}}$$

for $w = 0.1$ which is a reasonable approximation for small v. For small P one can see that

$$M \simeq M_0 \sqrt{\frac{1}{1 - \left(\frac{P}{M_0 c}\right)^2}}$$

where M_0 is the effective mass at $P = 0$. Since $M_0 \sim \frac{1}{\sqrt{\ell}}$ and $c \sim \sqrt{\ell}$ the curvature near $P = 0$ is decreasing with increasing ℓ, the size of the idle region.

4. Cherenkov radiation of Josephson fluxons

The usual sG equation is Lorentz invariant and fluxons can move without changing their shape and velocity. This is not the case for the non-local sG equation, where dispersion is introduced by the spatial non-locality. In this case fast moving fluxons can excite waves in the form of Cherenkov radiation [12]. To see this we consider propagating solutions and introduce a transformation to a frame of reference in which the centre of the fluxon is at rest [25]

$$\zeta = (z - vt)\gamma(v) \qquad \tau = \left(t - \frac{v}{c^2}z\right)\gamma(v) \qquad \gamma(v) = \frac{1}{\sqrt{1 - \frac{v^2}{c^2}}} \tag{39}$$

where v is the velocity of the fluxon. Applying this transformation to equation (12) we obtain for the phase $\Psi(\zeta, \tau)$

$$\gamma^2\frac{\ell}{c^2}\left(v^2\partial_\zeta^2-2v\partial_\zeta\partial_\tau+\partial_\tau^2\right)\Psi(\zeta,\tau)+2\gamma\hat{\kappa}(v)\tanh\left(\frac{\hat{\kappa}(v)\gamma\ell}{2}\right)\Psi(\zeta,\tau)=\frac{w}{\lambda_j^2}\sin\Psi(\zeta,\tau) \tag{40}$$

where the notation

$$\hat{\kappa}(v)=\sqrt{-\partial_\zeta^2+2\frac{v}{c^2}\partial_\zeta\partial_\tau-\frac{v^2}{c^4}\partial_\tau^2} \tag{41}$$

was used. We introduce perturbations around the stationary solution $\Phi(\zeta)$ from equation (12) in the form

$$\Psi(\zeta,\tau)=\Phi(\zeta)+f(\zeta,\tau) \tag{42}$$

where $f(\zeta,\tau)$ describes the change of the shape of the soliton and the radiation. Inserting equation (42) into equation (40) in the linear approximation for $f(\zeta,\tau)$ and using the Fourier transform of $f(\zeta,\tau)$

$$\bar{f}(k,\tau)=\frac{1}{2\pi}\int_{-\infty}^{\infty}\mathrm{d}\zeta\,\mathrm{e}^{-\mathrm{i}k\zeta}f(\zeta,\tau) \tag{43}$$

we obtain the linearized inhomogeneous differential equation

$$\gamma^2\frac{\ell}{c^2}\left(-2\mathrm{i}v\,k\partial_\tau+\partial_\tau^2\right)\bar{f}+\frac{\ell}{c^2}\Omega^2(k,v)\bar{f}+2\gamma\left[\hat{k}(v)\tanh\left(\frac{\gamma\hat{k}(v)\ell}{2}\right)-k\tanh\left(\frac{\gamma k\ell}{2}\right)\right]\bar{f}$$
$$-\frac{w}{\lambda_j^2}\overline{(1-\cos\Phi)f}=-2\mathrm{i}\left[\frac{\gamma^2v^2k\ell}{2c^2}-\gamma\tanh\left(\frac{\gamma k\ell}{2}\right)+\tanh\left(\frac{k\ell}{2}\right)\right]\overline{(\partial_\zeta\Phi)}(k) \tag{44}$$

where the operator $\hat{k}(v)$ is the extension of the operator $\hat{k}$ due to Lorentz transformation,

$$\hat{k}(v)=\sqrt{k^2+\mathrm{i}2\frac{vk}{v_j^2}\partial_\tau-\frac{v^2}{v_j^4}\partial_\tau^2} \tag{45}$$

that acts on the ζ-Fourier transform of $f(\zeta,\tau)$, and the function

$$\Omega(k,v)=\sqrt{\frac{v_j^2}{\lambda_j^2}\left[1+\frac{2\lambda_j^2}{w}k\gamma\tanh\left(\frac{k\gamma\ell}{2}\right)\right]-\gamma^2k^2v^2} \tag{46}$$

is the Swihart dispersion relation in the moving frame of reference. The left-hand side of equation (44) is the source of the radiation, which vanishes when $v=0$. The equation $\Omega(k,v)=0$ has two real roots at $k=\pm k_r$, which means that waves with wavenumbers $\pm k_r$ will be resonantly excited by a moving fluxon, forming an oscillatory tail [17, 27, 26]. For small fluxon velocities $v^2\ll c^2$, or equivalently $(\ell/w)\gg\left(v^2/v_j^2\right)$, the resonant wavenumber k_r and the corresponding frequency $\omega(k_r)$ can be expressed as

$$k_r\simeq\frac{2v_j^2}{wv^2} \tag{47}$$

$$\omega(k_r)=k_rv\simeq\frac{2v_j^2}{wv}. \tag{48}$$

In the resonant region $k\simeq\pm k_r$, we can neglect the second derivative ∂_τ^2f because, as will be seen later, the function f changes slowly in the interval $1/\omega(k_r)$:

$$|2\omega(k_r)\partial_\tau f|\gg\left|\partial_\tau^2f\right|. \tag{49}$$

We use the expansion of $\omega(k, v)$ around $k = \pm k_r$

$$\Omega^2(k, v) \simeq \mp 2vk_r(v - \partial_k\omega(k_r))(k \mp k_r) \simeq v^2 k_r(k \mp k_r) \tag{50}$$

and replace the right-hand side of equation (44) with its value at $k = k_r$. We also represent the function $\bar{f}(k, \tau)$ as a sum

$$\bar{f} = \bar{f}_+ + \bar{f}_- \tag{51}$$

where the function $\bar{f}_+$ ($\bar{f}_-$) differs from zero only in the close vicinity of the wave vector k_r ($-k_r$). Taking into account equations (49)–(51), we obtain from equation (44) that the functions $\bar{f}_\pm$ satisfy the equation

$$\mathrm{i}a\partial_\tau \bar{f}_\pm + \frac{v}{2}(k \mp k_r)\bar{f}_\pm \pm \frac{vw}{4\lambda_j^2}\overline{(1 - \cos\Phi) f_\pm} = \pi v a \frac{\cosh\left(\frac{k_r\ell}{2}\right)}{\cosh\left(\frac{\pi k_r \ell}{2\beta}\right)} \tag{52}$$

where the coefficient a is given by the expression

$$a = 1 - \frac{1}{k_r\ell}\left[\tanh\left(\frac{k_r\ell}{2}\right) + \frac{k_r\ell}{2}\mathrm{sech}^2\left(\frac{k_r\ell}{2}\right)\right]. \tag{53}$$

By virtue of equations (47) and (48) the second term on the right-hand side of equation (53) is small, thus we can put $a = 1$. Thus, returning to the real space (ζ, τ) we obtain from equation (52)

$$\partial_\tau f_\pm - \frac{v}{2}\partial_\zeta f_\pm \mp \frac{v}{2}\left(k_r + \frac{w}{2\lambda^2}(1 - \cos\Phi)\right) f_\pm = \pi v \frac{\cosh\left(\frac{k_r\ell}{2}\right)}{\cosh\left(\frac{\pi k_r \ell}{2\beta}\right)}\delta(\zeta). \tag{54}$$

With the initial condition $f(\zeta, \tau)|_{\tau=0} = 0$, the solution of equation (54) becomes

$$f = A\left[\theta\left(\zeta + \frac{v}{2}\tau\right) - \theta(\zeta)\right]\cos[k_r\zeta + \chi(\zeta)] \tag{55}$$

where the function

$$A = 4\pi \frac{\cosh\left(\frac{k_r\ell}{2}\right)}{\cosh\left(\frac{\pi k_r \ell}{2\beta}\right)} \tag{56}$$

is the amplitude of the radiation. The phase function $\chi(\zeta)$ has the form

$$\chi(\zeta) = \frac{w}{2\lambda^2}\int_0^\zeta \mathrm{d}\zeta(1 - \cos\Phi) = 2\arctan\left(\tanh\left(\frac{\zeta}{2}\right)\tan\left(\frac{\beta}{2}\right)\right). \tag{57}$$

It is seen that $|k_r\zeta| \gg \chi(\zeta)$ when $|\zeta| > 1$. Therefore we can neglect the phase function $\chi(\zeta)$ and returning to the original variables (z, t), we obtain that the radiation of the fluxon which moves with a velocity v is given by the function

$$f(z, t) = A\left[\theta\left(z - \frac{v}{2}t\right) - \theta(z - vt)\right]\cos(k_r z - \omega(k_r)t). \tag{58}$$

Thus, a moving fluxon stimulates radiation in the rear with a wavelength $\lambda = \frac{2\pi}{k_r} \sim v^2$. When the idle region is not wide, $\sqrt{w\ell} \ll \lambda_j$, while at the same time $\ell \gg w$, we obtain from equations (27) and (56) that the amplitude of the radiation can be expressed as

$$A(v \ll \lambda_j) = 4\pi \exp\left\{-\pi \frac{v_j^2}{v^2}\frac{w_f}{w}\right\} \tag{59}$$

where $w_f = \sqrt{\frac{\ell}{w}}\lambda_j$ is the fluxon width in the case of small non-locality. We see that the radiation increases when the fluxon width decreases. When the idle regions become very large ($\ell \to \infty$), the amplitude of the radiation takes the form

$$A(\ell \to \infty) = 4\pi \exp\left\{-4\frac{v_j^2}{v^2}\frac{\lambda_j^2}{w^2}\right\}. \tag{60}$$

In both cases the amplitude of the radiation decreases exponentially with decreasing fluxon velocity.

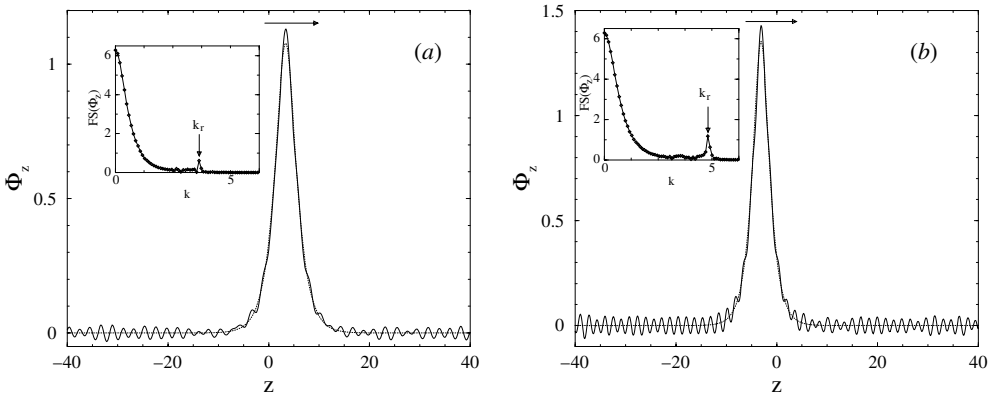

Figure 6. The propagating fluxon with the initial condition included as a dotted curve, and its corresponding Fourier spectrum in the inset (*a*) for $w = 0.1$, $\ell = 1.0$, $L = 80$ and $v = 2.5$ and (*b*) for $w = 0.2$, $\ell = 1.0$, $L = 80$ and $v = 1.6$.

5. Numerical results: radiation and Cherenkov steps

We solve equation (12) with periodic boundary conditions in the z-direction. The initial condition for the phases Φ is that obtained by the collective coordinate approach, with β calculated from equation (26). Assume that we have a travelling wave, $\Phi_t(z, t = 0) = -v\Phi_z(z, t = 0)$, with v taken from equation (29). For low velocity ($v \lesssim 1.6$) there is no radiation, and the coherent fluxons propagate in the junction for long time intervals without changing their shapes. Thus, the collective coordinate approach gives excellent results in this regime.

In figure 6(*a*) the propagating fluxon followed by radiation is shown for $v = 2.5$ (in units of v_j). The Fourier spectrum (the absolute value of the Fourier transform) of the waveform is shown in the inset of figure 6(*a*), where a peak due to the emitted radiation is evident, at $k = k_r \simeq 2.9$. In figure 6(*b*) we see another waveform and its Fourier spectrum (inset), for $w = 0.2$ and $v = 1.6$, while the other parameters remain the same as in figure 6(*a*). Notice that we increased the window width w from 0.1 to 0.2 in order to get stronger Cherenkov radiation. Indeed, we get stronger radiation in this case, as indicated by comparison of the peak values of figures 6(*a*) and (*b*), even though the fluxon motion is slower.

Even though the velocity v in both cases gets close to the corresponding $v_{\rm m}$ ($v_{\rm m} \simeq 1.95$ and $v_{\rm m} \simeq 2.80$ for figures 6(*a*) and (*b*), respectively) and appreciable radiation appears in the tails, the collective coordinates result (shown as dashed lines) still gives the correct trend for the fluxon profile.

For velocities very close to or higher than $v_{\rm m}$, however, the collective coordinate approach cannot be applied. Furthermore, the squared velocity becomes comparable with $c^2 = \ell/w$, and therefore the approximate analytical formulae for the radiation are not valid. In this regime, one has to resort to numerical simulations.

In order to make a connection with real Josephson junction arrays, we also included damping in the windows and driving current, which enters the junction from the end lines in the x-direction and is uniform in the z-direction (see figure 1). The equations for two junctions are obtained following the procedure of section 2, after adding a term of the form $-\gamma f(x)\partial_t\phi$ on the right-hand side of equation (2), with the modified boundary conditions

$$\phi_x(x = \pm(n\ell + \ell/2)) = \mp I/2. \tag{61}$$

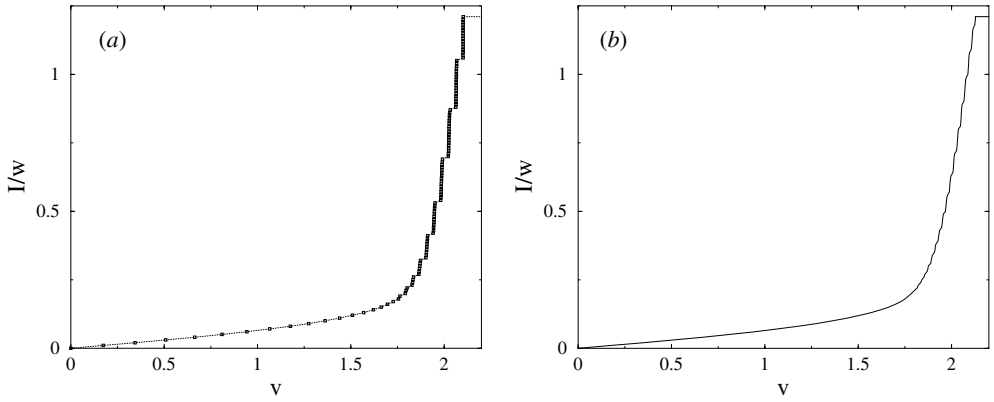

Figure 7. I–v characteristics for two coupled junctions with overlap current feed (a) for $w = 0.2$, $\ell = 1.0$, $L = 40$ and $\gamma = 0.05$ and (b) for $w = 0.2$, $\ell = 1.0$, $L = 80$ and $\gamma = 0.05$.

Then, considering only two junctions, we get (note that $\ell' = \ell/2$)

$$\partial_{tt}\bar{\Phi}_1 = -\frac{k}{w}\left[\tanh\left(\frac{k\ell}{2}\right) + \frac{1}{\tanh(k\ell)}\right]\bar{\Phi}_1 + \frac{k}{w\sinh(k\ell)}\bar{\Phi}_2 - \frac{I}{2w\cosh\left(\frac{k\ell}{2}\right)} - \overline{\sin\Phi_1} - \gamma\,\partial_t\bar{\Phi}_1 \tag{62}$$

where γ is the damping coefficient. The corresponding equation for Φ_2 is obtained by interchanging Φ_1 and Φ_2 in equation (62). Solving the coupled system of two equations for Φ_1 and Φ_2, the phases in windows 1 and 2, respectively, we confirm that the coherent solution is indeed stable. Inspection of the phases Φ_1 and Φ_2 shows that they are identical for any value of the driving current. The current–velocity (I–v) characteristics for the two coupled junctions biased on the first zero field step (ZFS) are shown in figure 7, where the current density per junction is $I/2w$. Notice that the fluxon velocity v is plotted on the horizontal axis, instead of the voltage $V = \frac{2\pi}{L}v$. The length of the junction $L = 40$ in figure 7(a), while $L = 80$ in figure 7(b), and the other parameters remain the same. At low velocities ($v \lesssim 1.25$) the I–v characteristics are linear and their slope is proportional to the damping coefficient γ. At higher velocities, however, the I–v characteristics acquire some curvature, and for $v \gtrsim 1.75$ fine structure in the form of substeps appears. These substeps are resonances due to strong interaction of the moving fluxons and the Cherenkov radiation, and usually they are referred to as Cherenkov steps.

Thus, if the junctions are biased on a Cherenkov step, one can increase the power of the emitted radiation while the radiation frequency remains constant by simply increasing the current within the range of the step. Similar resonances have been observed experimentally in a single window junction with lateral idle region [2], as well as in two long junctions in a stack [13, 14]. The resonances are much stronger for the shorter junction (figure 7(a)), where the Cherenkov steps are steeper, compared to those in figure 7(b). This is because in the shorter junction the radiation interference is much stronger with the fluxon and with itself, since it fills the whole junction. The resonance condition is imposed by the periodic geometry, that is, from the requirement that in a junction of length L, only an integer number of wavelengths are allowed, so that the wavevectors of the emitted radiation are given by $k_r = \frac{2\pi}{L}m$, where m is an integer. This also explains why the resonances are closely spaced together in the case of the longer junction. Obviously, the resonant k are twice as many as before, since the length L

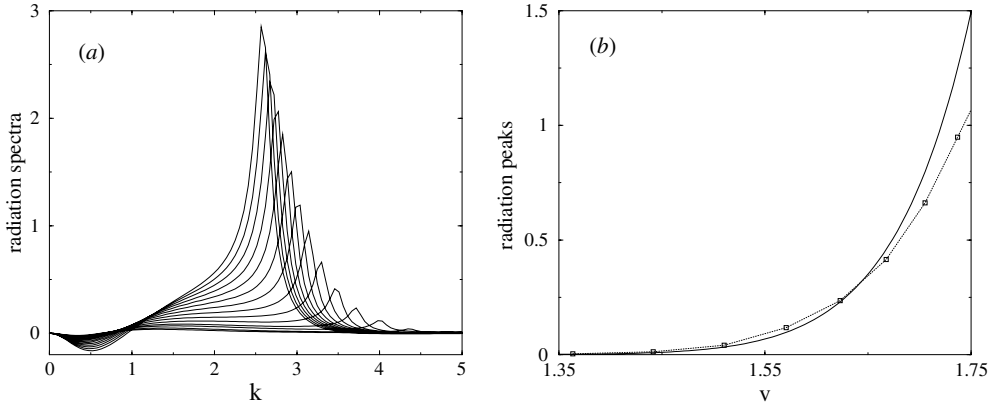

Figure 8. (*a*) The radiation spectra for several average velocities of the fluxon, for $w = 0.2$, $\ell = 1.0$, $L = 120$ and $\gamma = 0.1$. (*b*) The peak values of the spectra (squares) at $k = k_r$ for $w = 0.2$, $\ell = 1.0$, $L = 120$ and $\gamma = 0.1$, along with the theoretical values obtained as described in the text (solid curve). The dotted curve is a guide to the eye.

of the array has been doubled. Note also that in both cases the fluxons become unstable before reaching the maximum theoretical velocity, $c \simeq 2.24$, due to the resonant structure of the I–v curves.

In figure 8(*a*) the Fourier spectra of the radiation are shown, which are obtained by solving the coupled equations for two junctions, for several fluxon velocities v. In the driven and damped case, the fluxon velocity is determined by the external bias current. After taking the Fourier spectrum of the whole waveform, we have removed the Fourier spectrum of the fluxon, using the corresponding collective coordinate solution for each v. The maxima of these curves, which are related to the radiation amplitude, vary exponentially with $-1/v^2$, according to equation (56). For the parameters used in this figure ($L = 120$, $\ell = 1.0$, $w = 0.2$, $\gamma = 0.05$), the radiation gets damped by the time the fluxon makes the next round, and therefore the radiation cannot fill the whole junction. Thus, interference effects of the radiation with itself are absent.

In figure 8(*b*) we compare indirectly the radiation amplitudes obtained by numerical simulations and the theoretical formula. We assume that at some time t we have an integer number of periods for the radiation in the length L of the junction, in accordance with equation (58). Differentiating with respect to z we get $f_z = -k_r A \sin k_r(z - vt)$. Before taking the Fourier spectrum of f_z, we convolute this function with the exponential $\mathrm{e}^{-z/\delta}$, in order to take into account the decrease of the radiation behind the fluxon due to damping. The characteristic distance δ depends on the fluxon velocity. A reasonable estimation for δ is $\delta = v^2/2\gamma$, which gives, for the range of velocities of interest, $\delta \simeq 9$–16. The peaks of the Fourier spectra at $k = k_r$ are plotted versus the velocity v (solid curve) along with the numerically obtained ones (points connected with a dotted curve). We see that a fair agreement is obtained at low velocities.

In figure 9(*a*) we see that the points (k_r, ω), where k_r is the wavenumber of the emitted radiation (numerically determined from the peak of the spectra) and $\omega = vk_r$, fall very close to the analytic dispersion

$$\omega(k, q) = \frac{v_j}{\lambda_j}\sqrt{1 + \frac{2\lambda_j^2}{w}\frac{k}{\sinh k\ell}\left[\cosh(k\ell) - \cos(q\ell)\right]} \tag{63}$$

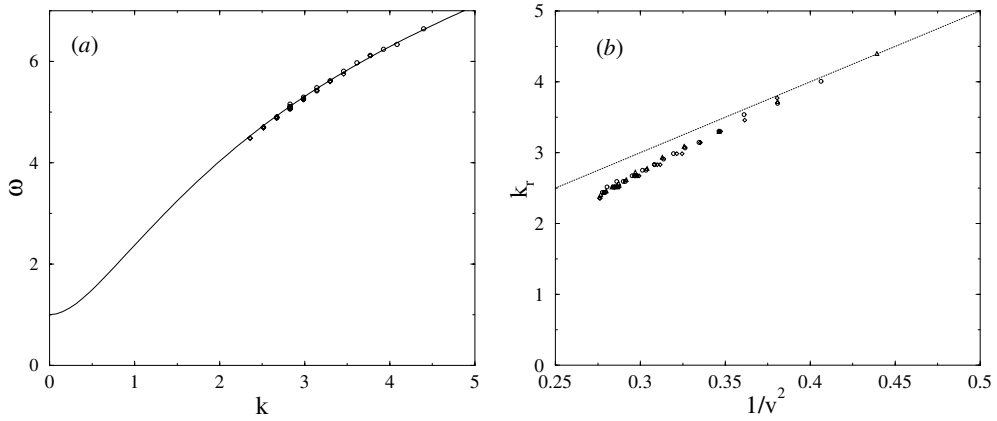

Figure 9. (*a*) The frequency of the emitted radiation $\omega = vk_r$ versus k_r for $w = 0.2$, $\ell = 1.0$, $L = 40$, $\gamma = 0.05$ (diamonds) and $\gamma = 0.075$ (circles), along with the analytic dispersion. (*b*) The wavenumber k_r versus $1/v^2$ for $w = 0.2$, $\ell = 1.0$, $\gamma = 0.05$ and $L = 40$ (diamonds), $L = 80$ (circles) and $L = 120$ (triangles). The dotted line is the theoretical prediction $k_r \simeq 2v_j^2/wv^2$.

where k and q are the longitudinal and transversal wavevectors, respectively ($q = 0$ for the lowest mode). We also see that the radiation frequency is independent of the damping, while in figure 9(*b*) we verify that $k_r \sim 1/v^2$ for three different junction lengths L. It turns out that k_r is also independent of the damping, that is, it depends only on the velocity v. For high velocities the overlapping same symbols come from resonant branches where the fluxon velocity is nearly constant but the current may vary significantly, without affecting the wavevector or the frequency of the emitted radiation.

6. Conclusions

We considered a planar superlattice of Josephson junctions coupled through intermediate linear (idle) regions, and we obtained the effectively non-local sG equations which describe the dynamics of that system. In the limit of very large idle regions ($\ell \to \infty$), we obtained the sine-Hilbert approximation with a long-range kernel. We studied the physically relevant solution of a coherent homopolar fluxon array. We applied the collective coordinate approach in order to obtain approximate analytic dynamic solutions in this case, which are valid up to a parameter-dependent velocity, $v_{\rm m}$. The relevant parameters of the trial function, β and $\dot{Z}$, are the inverse width and the fluxon position, respectively, which are constants at low velocities, resulting in uniform fluxon motion. They are determined by minimizing the effective potential $U_{\rm eff}$, which includes the magnetic energy along with the Josephson energy and the fluxon kinetic energy. From the analysis we see that the fluxon momentum P is the important parameter, since it is an integral of the motion. Thus, the correct prescription is to choose a value of P and determine the corresponding width and velocity from equations (26) and (29). There is fair agreement between the collective coordinate solutions and those obtained from direct numerical simulations using the non-local sG equation. The analysis was greatly facilitated by knowledge of the static solution of the non-local sG equation [16].

Well before the critical velocity $v_{\rm m}$ is reached, the Cherenkov radiation excited by the moving fluxons becomes significant. The emitted radiation appears as oscillations following the fluxon. We obtained analytical results for the wavevector, frequency, amplitude and the form of the emitted radiation, which also agree with the numerics, when $\frac{v^2}{c^2} \ll 1$. Surprisingly,

the collective coordinate solutions still give the correct trend as is also seen in numerical simulations. When the radiation is significant, the width of the junction will also be affected, starting to vary with time. In this case we also have the excitation of the fluttering mode which interferes with the radiation itself. The fluttering frequency $\omega_{\rm fl}$, obtained from numerical simulations also compares very well with the analytical result. At high velocities, one has to resort to numerical studies.

At low velocities the I–v characteristics do not depend on the junction length L. For short enough junctions, however, the radiation interferes much strongly with the fluxon and with itself since it covers the whole junction. Therefore, the Cherenkov steps seen at high velocities are steeper for the short junction.

At low velocities in the driven and damped case, the current is proportional to the fluxon velocity but also depends on the inverse width of the fluxon. Thus, even at low velocities the current depends on β/ℓ. For large ν values this can be a significant change over local models. Of course one could not explain the Cherenkov resonances at higher velocities within a local model. This possibility is very promising for the generation of coherent radiation with significant power output that will increase as the square of the number of junctions, N^2.

Acknowledgment

YBG would like to express his thanks for the hospitality of the University of Crete, where part of this work was done.

Appendix

From equation (20), after some simple algebra we get that

$$m'(\beta) = -\frac{\pi^2 w\ell}{3}\left(\frac{3}{\beta^4} + \frac{2}{\beta^3 \sin\beta}\right) - \frac{w\ell}{3}\left(\frac{2}{\beta \sin\beta} + \left(2 + \frac{\pi^2}{\beta^2}\right)\frac{\cos\beta}{\sin^2\beta}\right). \tag{A1}$$

Then for the coefficient $c(\beta) = m'(\beta)/m(\beta)$, we get

$$c(\beta) = -\frac{3}{\beta} + \left[\left(1 + \frac{6\beta^2}{\pi^2}\right) - \left(1 + \frac{2\beta^2}{\pi^2}\right)\frac{\beta\cos\beta}{\sin\beta}\right]\left[\sin\beta + \left(1 + \frac{2\beta^2}{\pi^2}\right)\beta\right]^{-1}. \tag{A2}$$

In the small β limit we can approximate $\sin\beta \simeq \beta$ and $\cos\beta \simeq 1 + \beta^2/2$, so that if we keep terms up to the first power in β we have

$$c(\beta) \simeq -\frac{3}{\beta} + c_0\beta \tag{A3}$$

with the constant

$$c_0 = \frac{1}{2}\left(\frac{4}{\pi^2} + \frac{1}{3}\right). \tag{A4}$$

In the same way for the effective mass we get

$$m(\beta) \simeq \frac{2\pi^2}{3}\left[\frac{1}{\beta} + \frac{1}{2}\left(\frac{1}{6} + \frac{2}{\pi^2}\right)\beta\right] \tag{A5}$$

where we also used $\beta = \sqrt{w\ell}$ in equation (20).

The first derivative of the potential $U(\beta)$ for the static case can be obtained from equation (25) as

$$U'(\beta) = \frac{\partial U}{\partial \beta} = \frac{4\beta}{\sin\beta} - \frac{w\ell}{\sin^2\left(\frac{\beta}{2}\right)} \tag{A6}$$

while its second derivative is

$$U''(\beta) = \frac{\partial^2 U}{\partial \beta^2} = 4\frac{\sin\beta - \beta\cos\beta}{\sin^2\beta} + \frac{w\ell\cos\left(\frac{\beta}{2}\right)}{\sin^3\left(\frac{\beta}{2}\right)} \tag{A7}$$

and their approximations for small β are

$$U'(\beta) \simeq \tfrac{1}{3}\beta^2 \tag{A8}$$

$$U''(\beta) \simeq \frac{8}{\beta} - \frac{8\beta}{3} \tag{A9}$$

where we kept terms up to β^2 in $U'_{\rm eff}(\beta)$ and used $w\ell \simeq \beta$ for small ℓ.

For the moving fluxon and finite β, we must use the Taylor expansion for $U_{\rm eff}$ around $\beta = \beta_p$. For $\beta = \beta_p + \delta$, with δ a small perturbation ($\delta \ll \beta_p$), we expand the effective potential around β_p (the minimum):

$$U_{\rm eff}(\beta) \simeq U_{\rm eff}(\beta_p) + \delta\frac{\partial U_{\rm eff}}{\partial\beta}\bigg|_{\beta=\beta_p} + \frac{1}{2}\delta^2\frac{\partial^2 U_{\rm eff}}{\partial\beta^2}\bigg|_{\beta=\beta_p} + \cdots$$

where $U_{\rm eff}$ is given by equation (25) and its derivatives are

$$U'_{\rm eff} = \frac{4\beta}{\sin\beta} - \frac{w\ell}{\lambda_j^2}\frac{1}{\sin^2\left(\frac{\beta}{2}\right)} - \frac{B^2}{2}\left\{\frac{1}{\beta^2} - \frac{1+\cos\beta}{(\beta+\sin\beta)^2}\right\} \tag{A10}$$

$$U''_{\rm eff} = 4\frac{\sin\beta - \beta\cos\beta}{\sin^2\beta} + \frac{w\ell}{\lambda_j^2}\frac{\cos\left(\frac{\beta}{2}\right)}{\sin^3\left(\frac{\beta}{2}\right)} - \frac{B^2}{2}\left\{-\frac{2}{\beta^3} + \frac{\sin\beta}{(\beta+\sin\beta)^2} + 2\frac{(1+\cos\beta)^2}{(\beta+\sin\beta)^3}\right\} \tag{A11}$$

where we added to equations (A6) and (A7) the contributions from the translational energy of the fluxon, and B^2 is given by

$$B^2 = \frac{4v^2}{c^2}\beta^2\left(1 + \frac{\beta}{\sin\beta}\right)^2 \equiv \frac{P^2\ell}{4w}v_j^2 = \frac{P^2c^2}{4}. \tag{A12}$$

At $\beta = \beta_p$ the potential has a minimum, thus $\frac{\partial U_{\rm eff}}{\partial\beta}\big|_{\beta=\beta_p} = 0$ and $U_{\rm eff}(\beta_p) = 0$. Thus the first non-zero term is $U_{\rm eff} = \frac{1}{2}\delta^2 U''(\beta_p)$, consequently

$$\frac{\partial U_{\rm eff}}{\partial\beta} \simeq \delta U''(\beta_p) = U''(\beta_p)(\beta - \beta_p)$$

. The differential equation for β becomes

$$\ddot{\beta} = -\frac{1}{2}\frac{3}{\beta}\dot{\beta}^2 - \frac{U''(\beta_p)}{m(\beta)}(\beta - \beta_p)$$

where we omitted the higher order term $c\beta\dot{\beta}^2$. For the effective mass $m(\beta)$, we used only the first term in equation (20), i.e. $m(\beta) \simeq 2\pi^2/3\beta$.

Introducing the small quantity $\delta = \beta - \beta_p$, we can write the equation of motion as

$$\ddot{\delta} = -\frac{1}{2}\frac{3}{\beta_p}\left(1 - \frac{\delta}{\beta_p}\right)\dot{\delta}^2 - \left(\frac{U''(\beta_p)}{m(\beta_p)}\right)\delta.$$

Dividing this equation by β_p we get

$$\frac{\ddot{\delta}}{\beta_p} = -\frac{3}{2}\frac{\dot{\delta}}{\beta_p}^2\left(1 - \frac{\delta}{\beta_p}\right) - \left(\frac{U''(\beta_p)}{m(\beta_p)}\right)\frac{\delta}{\beta_p}. \tag{A13}$$

By defining the quantity

$$\Delta = \frac{\delta}{\beta_p} \ll 1$$

we can rewrite equation (A13) as

$$\ddot{\Delta} = -\frac{3}{2}\dot{\Delta}^2(1-\Delta) - \left(\frac{U''(\beta_p)}{m(\beta_p)}\right)\Delta. \tag{A14}$$

Since $\Delta \ll 1$, we also have $\dot{\Delta} \ll 1, \ddot{\Delta} \ll 1$, and keeping terms up to $O(\Delta)$ we get the harmonic oscillator equation

$$\ddot{\Delta} = -\omega_{\text{fl}}^2 \Delta$$

where

$$\omega_{\text{fl}} = \sqrt{\frac{U''(\beta_p)}{m(\beta_p)}} \tag{A15}$$

is the so-called fluttering frequency. As a result of this frequency the fluxons have an oscillating width so that they have a breathing-like mode.

If the deviation is large, we must solve numerically for $\beta(t)$.

References

[1] Bindslev Hansen J and Lindelof P L 1984 *Rev. Mod. Phys.* **56** 431
[2] Monaco R, Pagano S and Costabile G 1988 *Phys. Lett.* A **131** 123
[3] Sakai S, Bodin P and Pedersen N F 1993 *J. Appl. Phys.* **73** 2411
[4] Sakai S, Ustinov A V, Kohlstedt H, Petraglia A and Pedersen N F 1994 *Phys. Rev.* B **50** 12905
[5] Benz S P and Burroughs C J 1991 *Appl. Phys. Lett.* **58** 2162
[6] van der Zant H S J, Berman D and Orlando T P 1994 *Phys. Rev.* B **49** 12945
[7] Holst T, Bindslev Hansen J, Groenbeck-Jensen N and Blackburn J A 1990 *Phys. Rev.* B **42** 127
[8] Carapella G, Costabile G and Sabatino P 1998 *Phys. Rev.* B **58** 15094
[9] Itzler M A and Tinkham M 1995 *Phys. Rev.* B **51** 435
[10] Caputo J G, Flytzanis N, Kurin V, Lazarides N and Vavalis E 1999 *J. Appl. Phys.* **85** 7282
[11] Franz A, Wallraff A and Ustinov A V 2001 *J. Appl. Phys.* **89** 471
[12] Flytzanis N, Lazarides N, Chiginev A, Kurin V and Caputo J G 2000 *J. Appl. Phys.* **88** 4201
[13] Goldobin E, Wallraff A, Thyssen N and Ustinov A V 1998 *Phys. Rev.* B **57** 130
[14] Goldobin E, Wallraff A and Ustinov A V 2000 *J. Low Temp. Phys.* **119** 589
[15] Hechtfischer G, Kleiner R, Ustinov A V and Muller P 1997 *Phys. Rev. Lett.* **79** 1365
[16] Gaididei Y, Lazarides N and Flytzanis N 2002 *J. Phys. A: Math. Gen.* **35** 10409
[17] Gaididei Yu B, Mingaleev S F, Christiansen P L and Rasmussen K Ø 1996 *Phys. Lett.* A **222** 152
[18] Matsuno Y 1995 *Int. J. Mod. Phys.* B **9** 1985
[19] Joseph R I 1977 *J. Phys. A: Math. Gen.* **10** L225
[20] Alfimov G L, Eleonsky V M, Kulagin N E and Mitskevich N V 1993 *Chaos* **3** 405
[21] Mints R G and Shapiro I 1994 *Phys. Rev.* B **49** 6188
[22] Alfimov G L and Silin V P 1995 *JETP* **81** 915
[23] Alfimov G L and Popkov A F 1995 *Phys. Rev.* B **52** 4503
[24] Genchev Z D 1997 *Supercond. Sci. Technol.* **10** 543
[25] Mingaleev S F, Gaididei Y B, Majerníková E and Shpyrko S 2000 *Phys. Rev.* B **61** 4454
[26] Kuehl H H and Zhang C Y 1990 *Phys. Fluids* B **2** 889
[27] Karpman V I 1993 *Phys. Rev.* E **47** 2073